ELSEVIER

Colloids and Surfaces
A: Physicochemical and Engineering Aspects 141 (1998) 119–130

COLLOIDS AND SURFACES A

Volume fraction effects in shear rheology and electroacoustic studies of concentrated alumina and kaolin suspensions

Stephen B. Johnson, Adrian S. Russell, Peter J. Scales *

Advanced Mineral Products Special Research Centre, School of Chemistry, University of Melbourne, Parkville 3052, Australia

Received 28 August 1997; accepted 17 November 1997

Abstract

The electroacoustic and shear yield stress response of concentrated alumina and kaolin suspensions have been measured across a range of pH conditions and volume fractions. The inter-relationship between the surface properties as measured electrokinetically and the shear yield stress is shown to scale in a straight forward manner for alumina particles and a qualitative description has been developed from kaolin suspensions. The pair-wise interaction between particles over the range of volume fractions has been demonstrated to remain constant. The use of a semi-empirical electroacoustic volume fraction correction to the zeta potential, integral to the electroacoustic technique, appears reasonable on the basis of the results presented herein. © 1998 Elsevier Science B.V.

Keywords: Electroacoustic; Shear yield stress; Alumina; Kaolin

1. Introduction

The interrelationship between surface chemistry and the corresponding bulk rheological properties is of importance to the processing of many colloidal suspensions. In particular, an understanding of this link allows manipulation of the compression, flow, filtration and dewatering behaviour of particulate systems to suit a wide variety of applications. An ideal circumstance would be one in which the rheological properties of a given system could be accurately determined from the measurement of its electrokinetic and particle size characteristics, or vice versa. Unfortunately, despite the attentions of a number of workers in recent years, the quantification of the surface chemistry–rheology association has remained largely unresolved. Of those treatments currently available, many require the estimation of parameters whose form is neither physically obvious nor experimentally determinable, or else invoke the use of materially meaningless empirical fitting constants whose presence undermine the integrity of the modelling process.

The model of Scales et al. [1] recently developed from that of Kapur et al. [2] represents a fresh approach in attempting to describe the static shear rheological behaviour of simple particulate suspensions across the pH range solely from experimentally ascertainable parameters. For a polydisperse suspension of spherical particles, a general expression for the shear yield stress, τ_y, is [2]

$$\tau_y = \frac{1}{6}\sum_j n_j \sum_i K_{ij} H_{ij} \quad (1)$$

* Corresponding author. Tel: 61-3-93446480;
Fax: 61-3-93446233;
e-mail: p.scales@chemistry.unimelb.edu.au

PII S0927-7757(98)00208-8

where

$$n_j = \frac{6\phi}{\pi X_j^2} S_j, \tag{2}$$

$$K_{ij} = S_i K_{ij}(b) \tag{3}$$

and

$$K_{ij}(b) = 0.134K(\phi)\left[\frac{\frac{Xj}{Xi}+1}{1+\frac{X_j}{X_i}-\sqrt{\frac{X_j}{X_i}\left(\frac{Xj}{Xi}+2\right)}}\right]. \tag{4}$$

X_i and X_j are the mean diameters of particles residing in the i-th and j-th size intervals. S_i and S_j are the fractions of the total surface area contributed by particles of diameter X_i and X_j, respectively. K_{ij} and $K(\phi)$ are the mean coordination numbers of spherical particles comprising a monodisperse and a polydisperse suspension, respectively. H_{ij} is the mean interaction force between two particles of diameters X_i and X_j.

In defining H_{ij}, the mean interaction force was assumed to be given by the sum of the attractive van der Waals and repulsive electrical double layer forces (DLVO theory [3]). The van der Waals' interaction between two particles of size X_i and X_j may be calculated from

$$H_{ij} = \frac{A_H}{12h_0^2}\left[\frac{X_i X_j}{X_i + X_j}\right], \tag{5}$$

where A_H is the Hamaker constant of the colloidal material and h_0 is the inter-particle separation for particles flocculated to a primary minimum.

Assuming both that the electrical double layer potentials satisfy the Debye–Hückel condition and that the particles follow constant surface potential behaviour as a function of inter-particle separation, the Hogg–Healy–Fuerstenau (HHF) [4] expression for the electrical double layer interaction is applicable. For the interaction of two particles of size X_i and X_j, this is

$$H_{ij} = -\frac{4\pi\epsilon\epsilon_0\kappa\zeta^2}{2(1+e^{\kappa h_0})}\left[\frac{X_i X_j}{X_i + X_j}\right], \tag{6}$$

where ζ is the electrokinetic zeta potential, κ^{-1} is the characteristic Debye length, ϵ is the dielectric constant of the bulk suspending medium, and ϵ_0 is the permittivity of a vacuum.

Combining Eqs. (1)–(6) allows derivation of the expression [2]

$$\tau_y = \frac{0.011}{\pi}\phi K(\phi)\left[\frac{A}{h_0^2} - \frac{24\pi\epsilon\epsilon_0\kappa\zeta^2}{(1+e^{\kappa h_0})}\right]\sum_j \frac{S_j}{X_j}\sum_i \times S_i\left[\frac{X_i}{(X_j+X_i)-\sqrt{X_j^2+2X_iX_j}}\right]. \tag{7}$$

For a monodisperse particle system, this reduces to the simple form

$$\tau_y = \frac{0.022}{\pi X}\phi K(\phi)\left[\frac{A}{h_0^2} - \frac{24\pi\epsilon\epsilon_0\kappa\zeta^2}{(1+e^{\kappa h_0})}\right]. \tag{8}$$

As the van der Waals and electrical double layer force expressions were originally derived for interactions between two particles, Eqs. (7) and (8) are based on the supposition that the shear yield stress is simply equivalent to the pair-wise summation of all interactions between the primary particles within the suspension. Such an assumption is questionable, however, in view of recent developments involving the fractal type analysis of Potanin et al. [5,6]. Under this treatment, the aggregate structure of weakly flocculated colloidal dispersions is envisaged as a series of networked chains of varying elasticity and rigidity. The result is a series of weak links which will inelastically deform under less strain than those associated with the rigid networks. An alternative analysis is to view the system as a series of weakly interconnected aggregate structures compromising strongly interacting primary particles. Clearly in such a system the weak inter-floc links would yield under a lower strain than those within the aggregate. The result is an experimental yield stress that is lower than that predicted by Eqs. (7) and (8) unless the volume fraction is such that the ratio of weak to strong links is low. This has been shown to occur at high volume fractions, with the required volume fraction decreasing with decreasing particle size [7]. The average coordination number under such conditions should be only weakly compromised by

the floc structure, and a number of theoretical forms have been hypothesized [8,9].

In order to move away from the complicating structural factors outlined above, Eqs. (7) and (8) may be normalized against the result at the electrokinetic isoelectric point; that is, when the ζ-potential is zero and the static shear yield stress is at its maximum, τ_{ymax}. The resulting expression is [2]

$$\frac{\tau_y}{\tau_{ymax}} = 1 - \frac{24\pi\epsilon\epsilon_0\kappa\zeta^2 h_0^2}{A[1+e^{\kappa h_0}]}. \quad (9)$$

Eq. (9) allows prediction of the form, but not the absolute value, of the static shear yield stress independently of the structural properties of the suspension, i.e. the particle size and coordination number. Preliminary studies [2] on a simple model alumina suspension have yielded promising results. In that case, the normalized shear yield stress curves were found to be identical across the range of volume fractions studied. In addition, h_0 was found to be independent of both volume fraction and ζ-potential across the pH region where the yield stress was non-zero. The method used to determine h_0 in the previous study was, however, relatively insensitive, and prone to some degree of subjectivity on behalf of the analyser.

The purpose of this work is to revisit the original alumina data and demonstrate a more objective method of determining h_0. The more complex case of a kaolin system is then considered, with the aim of comparing the relationship between surface chemistry and rheology for a heterogeneously charged plate-like as distinct from a homogeneously charged spherical particulate system. The results provide a unique insight into the surface chemistry–shear rheology interrelationship for non-spherical particle suspensions.

2. Experimental section

High purity AKP-30 alumina was obtained from Sumitomo Chemical Co., Japan. It had a BET surface area of 7 $m^2\,g^{-1}$, a mean primary particle diameter of ca. 0.3 μm, and was shown by transmission electron microscopy to consist more of oblong than spherical shaped particles with an aspect ratio less than 2:1. Acid-washed kaolin was obtained from Ajax Chemicals. Transmission electron microscopy confirmed the presence of hexagonal plate-like particles with a mean face diameter of ca. 1 μm. The BET surface area was found to be 14 $m^2\,g^{-1}$. Water used in this study was distilled before ultra-purification with charcoal and ion-exchange resins (Milli-Q: conductivity $<1\times10^6\ \Omega^{-1}cm^{-1}$ at 20°C). A background electrolyte concentration of 0.01M KNO_3 was employed in all cases. The suspension pH was adjusted using analytical grade HNO_3 and KOH.

For all experiments, samples were prepared by sonicating a suspension of the desired volume fraction under dispersed conditions for 1 min with a Branson B-30 sonifier. The sonifier was operated at a frequency of 20 kHz and with the power output between 50 and 60% of the maximum power (350 W). The samples were allowed to stand for at least 2 h prior to measurement. All experiments were conducted with the pH progressing from acidic to basic solution conditions.

The electrophoretic mobility was determined using both a Rank Brothers Mark 11 and a Coulter Delsa 440 electrophoresis apparatus. The electrophoretic zeta potential was then calculated using the algorithm of O'Brien and White [10]. The electroacoustic dynamic mobility and zeta potential was determined using an Acoustosizer instrument (Matec Applied Sciences). This instrument applies a high frequency alternating voltage to the colloidal suspension, causing the particles to oscillate at a velocity that is dependent upon their size and zeta potential. The resulting pressure forces that arise at the suspension boundaries produce pulses of sound waves in a phenomenon known as the electrokinetic sonic amplitude (ESA) effect. For an isotropic colloidal suspension of volume fraction $\phi<0.02$, the ESA signal is related to the particle-averaged dynamic mobility, $\langle\mu_D\rangle$, by the expression [11]

$$ESA(\omega) = F(\omega)\phi\,\frac{\Delta\rho}{\rho}\langle\mu_D\rangle, \quad (10)$$

where ω is the angular frequency of the applied field, F is an instrument constant, ρ is the suspending medium density, and $\Delta\rho$ is the density differ-

ence between the colloidal component and the suspending medium.

For the case of a spherical particle with a thin double layer, negligible surface conductance and relatively low dielectric permittivity, μ_D can be related to the ζ-potential by the relationship [12]

$$\mu_D = \frac{\epsilon\zeta}{\eta} G(\alpha), \tag{11}$$

where ϵ and η are the viscosity and permittivity of the suspending medium respectively. $G(\alpha)$ is a complex inertial term dependent upon the particle size and density.

The Acoustosizer instrument measures the ESA signal over 13 frequencies from 0.30 to 11.15 MHz, with the results being signal averaged. Measurements were not possible within two pH units of the isoelectric point (iep) of alumina suspension above 20 vol.% (v/v%) or for kaolin suspensions above 18 v/v%. This was presumably due to incorporation of air pockets into solution, including around the electrodes, through the action of the stirrer under highly viscous suspension conditions.

The static shear yield stress was measured using the vane technique of Nguyen and Boger [13,14]. Following this method, a four bladed vane was slowly immersed in the suspension and rotated at very low shear rate (0.2 rpm). The applied torque was monitored, and the maximum torque, F_{max}, related to the static shear yield stress by [14]

$$F_{max} = \frac{\pi D_v^3}{2}\left(\frac{H_v}{D_v} + \frac{1}{3}\right)\tau_y \tag{12}$$

where D_v and H_v are the diameter and height of the vane respectively.

3. Results and discussion

3.1. Alumina suspensions

For suspensions of arbitrary volume fraction, Rider and O'Brien [15,16] have defined the dynamic mobility as

$$\langle U\rangle = \mu_D\langle E\rangle + \gamma\mathbf{u} \tag{13}$$

where $\langle E\rangle$ is the mean applied electric field, $\langle U\rangle$ is the mean particle velocity, γ is the particle sound wave mobility, related to the acoustic properties of the suspension, and **u** is defined as the macroscopic momentum per unit mass, created by the local bulk motion of the suspension. At high solids concentrations, where particle interactions become significant, the dynamic mobility is reduced by interactions between the hydrodynamic and electrical field disturbances around each particle.

The above effect is demonstrated for AKP-30 alumina in Fig. 1(a),(b), where the dynamic mobility as a function of pH at both low (0.42 MHz) and high (11.15 MHz) frequencies is observed to decrease in magnitude as the solids volume fraction is increased.

The corresponding effect upon the calculated electrokinetic ζ-potential is shown in Fig. 2. Again, the apparent ζ-potential is seen to decrease significantly with increasing solids concentration in the pH region of interest. Importantly, however, the position of the electrokinetic isoelectric point remains constant at pH 9.4, and is in good agreement with previous findings for alumina-based systems [17–19].

Unfortunately, the derived corrections to the dynamic mobility due to γ and **u** are mathematically complex, and applicable only for suspensions of monodisperse spherical particles [15,16]. A far more simplistic approach is therefore to apply an empirical correction to the zeta potential data obtained for concentrated suspensions in order to adjust it to its low volume fraction limit. This procedure is valid provided one or both of the following conditions apply:

- the extent of electrical double layer overlap is low;
- the particles approximate constant surface potential behaviour as a function of interparticle separation in the case of significant electrical double layer overlap.

The Acoustosizer instrument uses a semi-empirical correction based upon previous measurements involving metal oxide systems [20]. This correction is assumed to be applicable in this case. The form of this correction (R.W. O'Brien, Colloid Dynamics Ltd, pers. comm.) is

$$\zeta_{corr} = \zeta_{app}\exp\{2\phi[1+s(\phi)]\} \tag{14}$$

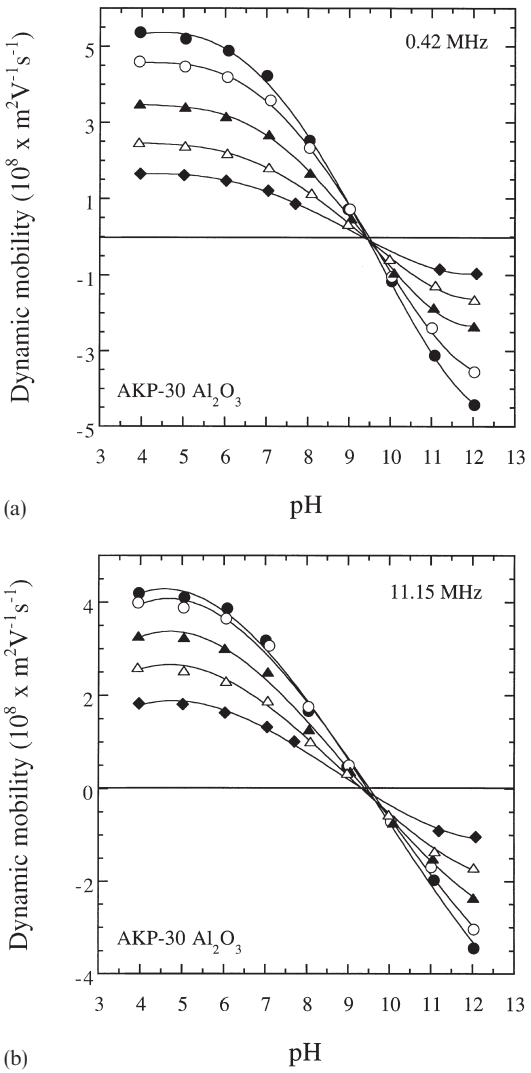

Fig. 1. The dynamic mobilities of AKP-30 alumina suspensions as a function of both volume fraction and pH. The presented results were measured at frequency (a) 0.42 MHz and (b) 11.15 MHz. ●, $\phi=0.020$; ○, $\phi=0.060$; ▲, $\phi=0.120$; △, $\phi=0.200$; ◆, $\phi=0.300$.

where

$$s(\phi)=\left[1+\left(\frac{0.1}{\phi}\right)^4\right]^{-1}. \quad (15)$$

ζ_{app} and ζ_{corr} are the apparent measured and corrected ζ-potentials respectively.

Fig. 3 shows the effect of applying Eqs. (14) and (15) to the zeta potential data presented in Fig. 2.

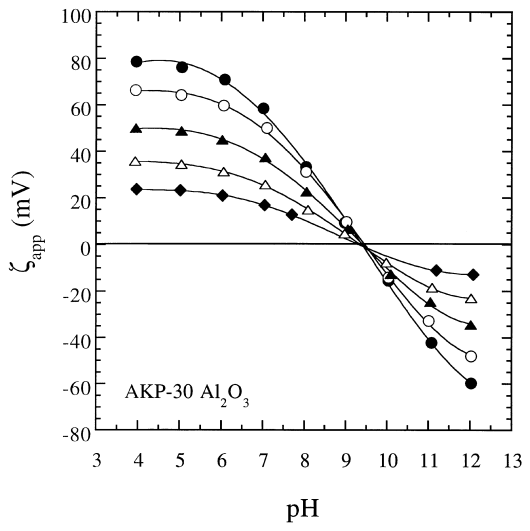

Fig. 2. The variation of the apparent (measured) ζ-potential, ζ_{app}, of AKP-30 alumina suspensions with both volume fraction and pH. ●, $\phi=0.020$; ○, $\phi=0.060$; ▲, $\phi=0.120$; △, $\phi=0.200$; ◆, $\phi=0.300$.

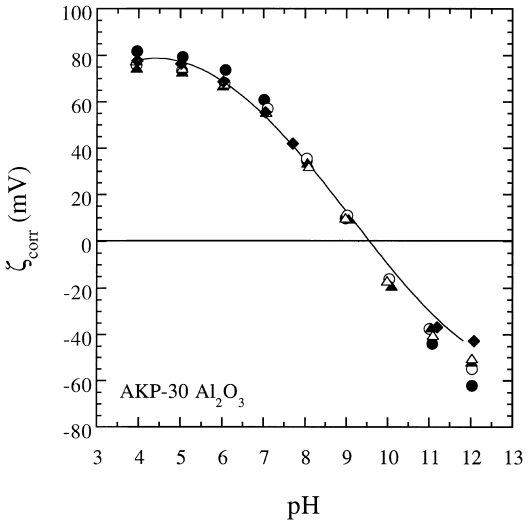

Fig. 3. The semi-empirically corrected ζ-potential, ζ_{corr}, of AKP-30 alumina suspensions as a function of both volume fraction and pH. The line plot is representative of ζ-potentials obtained from d.c. electrophoresis data. ●, $\phi=0.020$; ○, $\phi=0.060$; ▲, $\phi=0.120$; △, $\phi=0.200$; ◆, $\phi=0.300$.

All values of ζ_{corr} are seen to lie within *ca.* 10 mV of the low solids concentration ($\phi=0.02$) data over the pH range. The corrected ζ-potentials are also demonstrated to be in excellent agreement with

data obtained at extreme dilution via electrophoresis ($\phi = 1 \times 10^{-5}$), as shown by the solid line in Fig. 3. It is noteworthy, however, that while the above semi-empirical correction appears reasonable for metal oxide systems, it is not universally applicable, having been noted to substantially overcorrect for near neutrally buoyant colloids (A.S. Russell, University of Melbourne, unpublished data, and [21]).

The raw and normalized static shear yield stresses of AKP-30 alumina suspensions as a function of volume fraction and pH are shown in Fig. 4(a),(b), respectively. The parabolic nature of the curves shows good correlation of the maximum in the yield stress and the isoelectric point as determined electrokinetically. The shape is consistent with the concept that a maximum in the rheology occurs for a maximum in the net inter-particle force. The normalized yield stress data is observed to collapse onto a single curve, and has previously been fit to Eq. (9) assuming a Hamaker constant of 5.3×10^{-20} [22], a volume–fraction independent ζ-potential as provided by Eqs. (14) and (15), and a mean inter-particle separation, h_0, of 23 Å [2].

Quantification of h_0 may be undertaken in a more sensitive manner by plotting the normalized static shear yield stress against ζ^2, as shown in Fig. 5. The result is a linear relationship whose gradient is dependent only upon h_0. Fig. 5 demonstrates the data for all volume fractions to fit a h_0 value of 23–24 Å, in good agreement with that previously determined. Lines corresponding to $h_0 = 14$ Å and $h_0 = 34$ Å are also displayed to indicate the sensitivity of this method. The finding of a linear relationship between the normalized shear yield stress and ζ^2 is in agreement with those earlier observations of Hunter and Nicol [23] and Firth [24], the difference being that normalization of the data allows a quantitative assessment of the inter-particle spacing and assessment of the uniformity of the inter-particle force as a function of volume fraction. The effect of parameters such as surface roughness on the value of h_0 is unknown at this point in time. It is clear that the particles are in a primary minimum in a DLVO sense since there is no barrier to coagulation for potentials of magnitude less than 30 mV. At higher salt concentrations, such a separation distance would

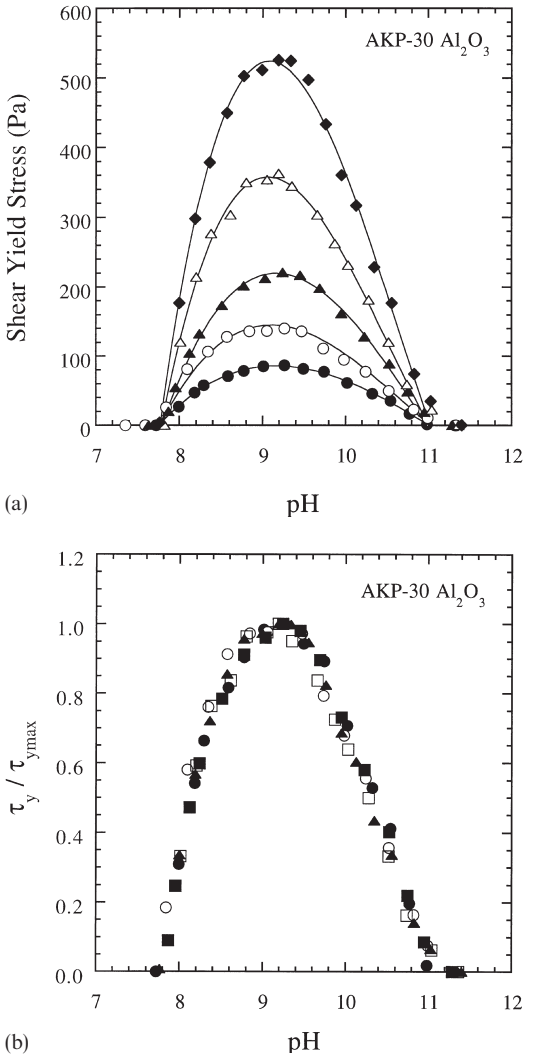

Fig. 4. The (a) measured and (b) normalized static shear yield stress of AKP-30 alumina suspensions as a function of both volume fraction and pH. ●, $\phi = 0.200$; ○, $\phi = 0.225$; ▲, $\phi = 0.250$; △, $\phi = 0.275$; ◆, $\phi = 0.300$.

constitute the extent of the electrical double layer and comparison of the value of h_0 calculated here with that from studies of macroscopically smooth surfaces, as for say muscovite mica, is an interesting topic for future research.

3.2. Kaolin suspensions

Understanding the surface chemistry and rheology of kaolin suspensions is complicated greatly

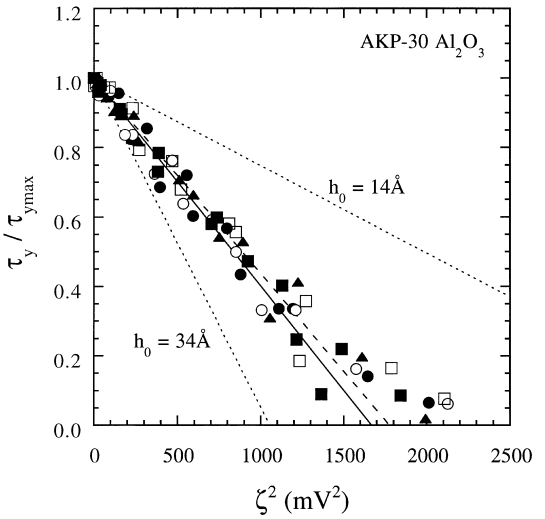

Fig. 5. The normalized static shear yield stress as a function of ζ^2 for several AKP-30 alumina suspensions. The two central line plots correspond to $h_0=23$ Å (- - -) and $h_0=24$ Å (———) respectively, as calculated using Eq. (9). Line plots corresponding to $h_0=24$ Å and $h_0=34$ Å are additionally given to show the sensitivity of the gradient to the inter-particle separation. ●, $\phi=0.200$; ○, $\phi=0.225$; ▲, $\phi=0.250$; △, $\phi=0.275$; ◆, $\phi=0.300$.

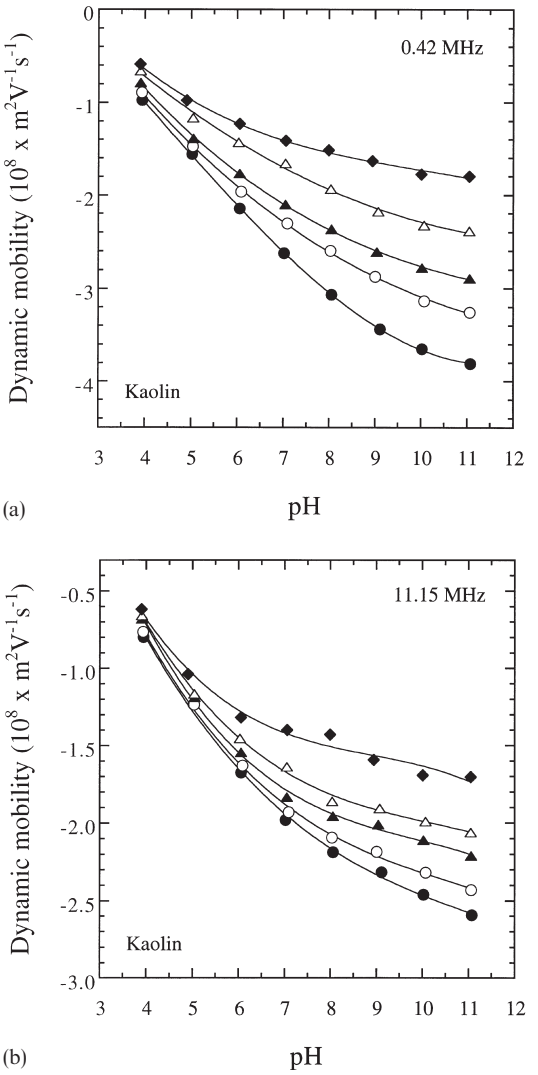

Fig. 6. The dynamic mobilities of Ajax kaolin suspensions as a function of both volume fraction and pH. The results displayed were measured at frequency (a) 0.42 MHz and (b) 11.15 MHz, respectively. ●, $\phi=0.200$; ○, $\phi=0.060$; ▲, $\phi=0.090$; △, $\phi=0.130$; ◆, $\phi=0.180$.

both by the presence of heterogeneously charged edges and faces on each particle, and by the plate-like particle nature. The kaolin edges contain both silica and alumina-like sites. They are positively charged at low pH, but progress through an isoelectric point at ca. pH 7 [25,26] to possess a negative charge at high pH. By contrast, the kaolin face contains only silica-like charge sites, and remains negatively charged across the pH range. A substantial proportion of the overall face negative charge is believed to originate from isomorphous ion substitution of Mg^{2+} for Al^{3+} in the alumina octahedral layer and, to a lesser extent, Al^{3+} for Si^{4+} in the silica tetrahedral layer of the lattice [27].

In practice, the electrokinetic characteristics of kaolin suspensions are anticipated to be dominated by the charge properties of the crystal face due to the large face-to-edge surface area ratio. This expectation is borne out by the data of Fig. 6, which demonstrates the electroacoustic dynamic mobilities to be negative across the pH range of interest for all volume fractions investigated. As was the case for the alumina data, failure to take account of the acoustic and macroscopic momentum properties of the suspension at volume fractions where particle interactions are significant results in a marked decrease in the magnitude of the dynamic mobilities and ζ-potentials as the solids volume fraction increases (Figs. 6 and 7).

Fig. 8 shows the ζ-potentials obtained after cor-

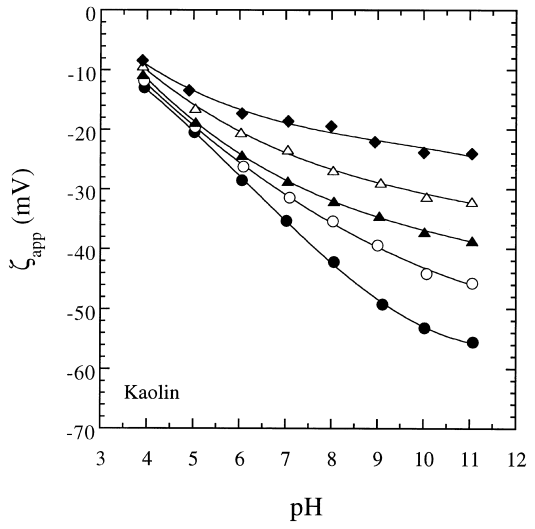

Fig. 7. The variation of the apparent (measured) ζ-potential, ζ_{app}, of Ajax kaolin suspensions with both volume fraction and pH. ●, $\phi=0.200$; ○, $\phi=0.060$; ▲, $\phi=0.090$; △, $\phi=0.130$; ◆, $\phi=0.180$.

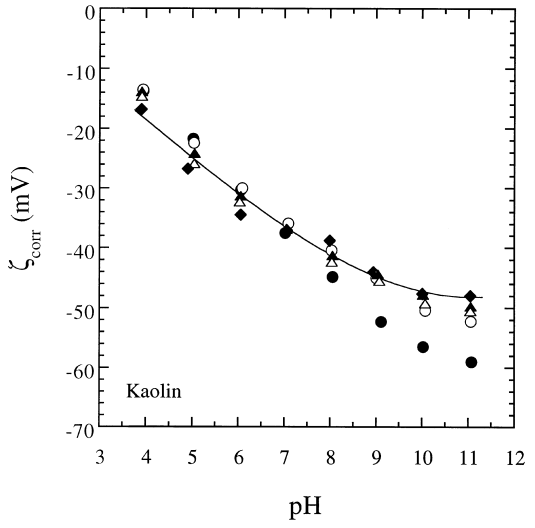

Fig. 8. The semi-empirically corrected ζ-potential, ζ_{corr}, of Ajax kaolin suspensions as a function of both volume fraction and pH. The line plot is representative of ζ-potentials obtained from d.c. electrophoresis data. ●, $\phi=0.200$; ○, $\phi=0.060$; ▲, $\phi=0.090$; △, $\phi=0.130$; ◆, $\phi=0.180$.

rection using the semi-empirical approach set out in Eq. (15). All values of ζ_{corr} are seen to be in reasonable agreement with the low volume fraction data until *ca.* pH 9. A similar agreement is noted with the zeta potentials from electrophoresis data (solid line) until this point. Beyond pH 9, significant deviations of the low volume fraction ($\phi=0.02$) data from that of both the more concentrated systems and the electrophoresis results are observed. The reasons for this discrepancy is unknown at this stage. For the purposes of further discussion in this paper, the intermediate $\phi=0.12$ data will be used due to its greater consistency with the electrophoretic zeta potentials given in Fig. 8.

The shear yield stress and normalized shear yield stress of the kaolin suspension as a function of pH and volume fraction is shown in Fig. 9(a),(b). The normalized data collapse onto a single curve as for the alumina case. However, the observed yield stress maxima show no obvious correlation with the electrokinetic zeta potential data. In addition, the relationship of the normalized static shear yield stress with ζ^2 is clearly non-linear (Fig. 10).

A mathematical description of the static shear yield stress behaviour of kaolin requires major modifications to the previously espoused model. These include consideration of interactions between planar surfaces of finite thickness as opposed to spherical interfaces. In addition, the treatment must be able to take account of edge-edge, face-face and edge-face interactions. In the latter case, this involves modifying the electrical double layer treatment to allow for interaction of dissimilarly charged surfaces.

An appropriate form for the van der Waals force between two planar surfaces of thickness δ is [28]

$$H=\frac{A_H}{12\pi}\left[\frac{1}{h_0^2}+\frac{1}{(h_0+2\delta)^2}-\frac{2}{(h_0+\delta)^2}\right] \qquad (16)$$

The electrical double layer force between two planar surfaces with zeta potentials ζ_1 and ζ_2 is given by the HHF expression for dissimilarly charged surfaces, namely [4]

$$H=-\epsilon\epsilon_0\kappa^2\,\mathrm{cosech}\frac{(\kappa h_0)}{2}\,[(\zeta_1^2+\zeta_2^2)\,\mathrm{cosech}(\kappa h_0) -2\zeta_1\zeta_2\coth(\kappa h_0)]. \qquad (17)$$

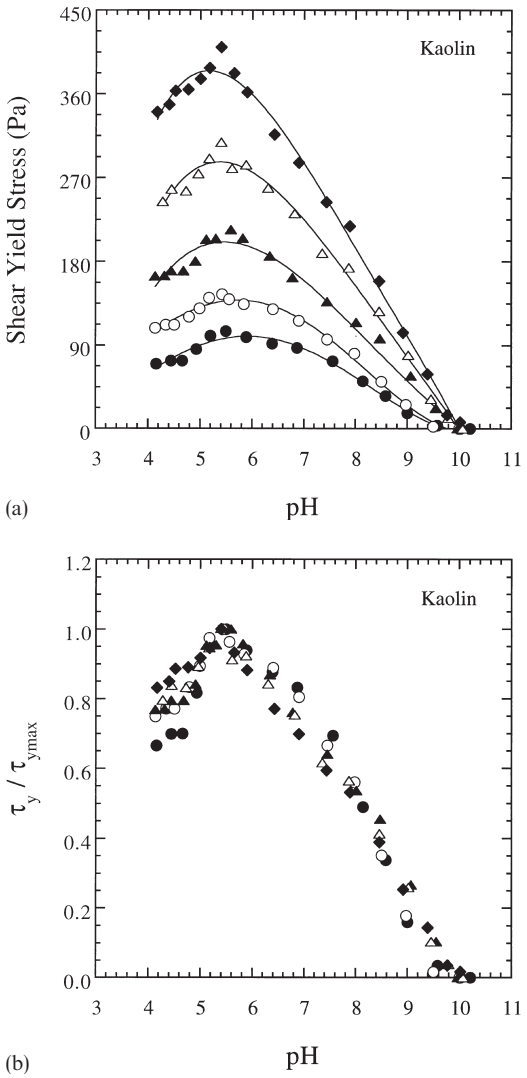

Fig. 9. The (a) measured and (b) normalized static shear yield stress of Ajax kaolin suspensions as a function of both volume fraction and pH. ●, $\phi=0.180$; ○, $\phi=0.200$; ▲, $\phi=0.220$; △, $\phi=0.240$; ◆, $\phi=0.260$.

In cases where ζ_1 and ζ_2 are identical, as for face-face and edge-edge interactions, Eq. (17) reduces to

$$H=\epsilon\epsilon_0\kappa^2\zeta^2\ \mathrm{cosech}(\kappa h_0)[\mathrm{cosech}(\kappa h_0)-\coth(\kappa h_0)]. \quad (18)$$

In order for the above treatment to be useful, resolution of the net kaolin electrokinetic behaviour into its edge and face components is required. One experimental method by which this may be achieved is to negate either the edge or face charge by adsorption of an appropriate surface active species. The measured electrokinetic behaviour is then governed solely by the remaining charged surface. Unfortunately this process proves to be extremely difficult in practice due to the presence of both positive (alumina-like) and negative (silica-like) sites on the kaolin edge surface. Attempts to negate the face charge by adsorption of positively charged species will therefore affect the negative edge charge sites, while adsorption of an anionically charged species to the edge will leave a residual negative edge charge. This problem was considered by Williams and Williams [25], who approximated the edge potential in the presence of a number of 1:1 electrolyte concentrations by addition of α-alumina and quartz data. Given an aspect ratio of ca. 10:1 for the kaolin particles, correction of the overall zeta potential (Fig. 8) with the data of Williams and Williams allows determination of the likely face potential. The result is given in Fig. 11.

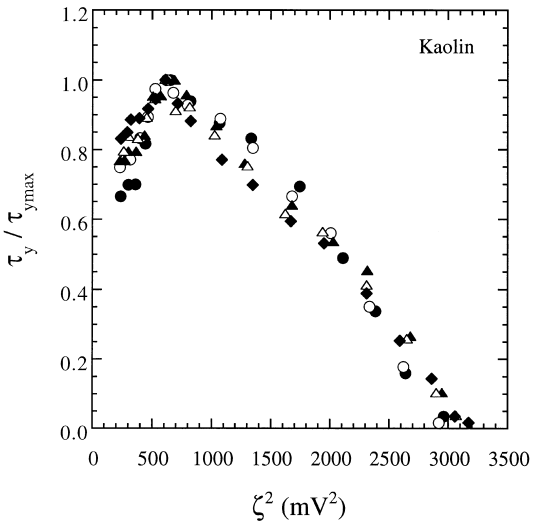

Fig. 10. The normalized static shear yield stress as a function of ζ^2 for Ajax kaolin suspensions. ●, $\phi=0.180$; ○, $\phi=0.200$; ▲, $\phi=0.220$; △, $\phi=0.240$; ◆, $\phi=0.260$.

Fig. 12 shows the relative net force of interaction for edge-face, face-face and edge-edge interparticle orientations, where the force has been

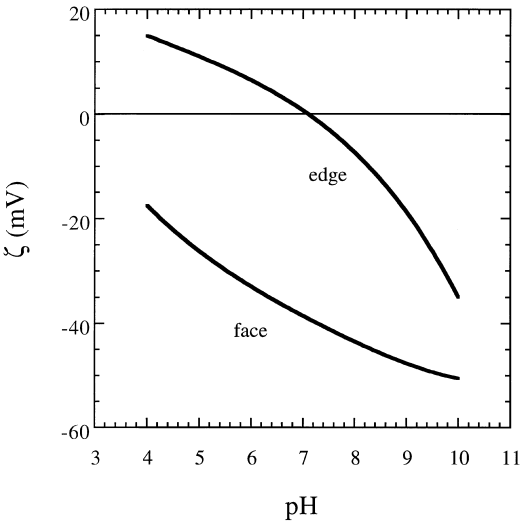

Fig. 11. The electrokinetic behaviour of the kaolin edge and face respectively in the presence of 10^{-2} M background electrolyte. Edge data was taken from [25]. Face ζ-potentials were determined by correcting the combined experimental data (Fig. 9) for the effect of the edge ζ-potential.

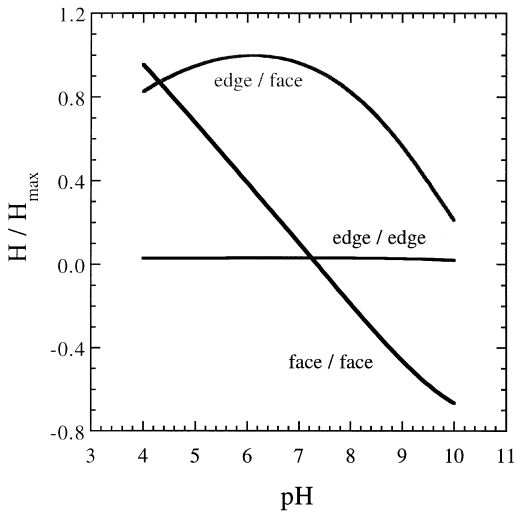

Fig. 12. The predicted kaolin edge-face, face-face and edge-edge interaction forces scaled relative to the maximum attractive edge-face force, and multiplied by the effective interaction area to simulate the rheological response. Hamaker constants of 8.5×10^{-21}, 1.8×10^{-20} and 1.3×10^{-20} were used in calculation of face-face, edge-edge and edge-face interaction forces respectively. An inter-particle separation of $h_0=20$ Å was used in all calculations.

multiplied by the predicted interaction area ratio of 18:81:1. The forces are scaled against the maximum predicted edge-face interaction force, H_{max}. A silica–silica Hamaker constant of 8.5×10^{-21} [22] was used in calculation of face-face interaction forces. The Hamaker constant of 1.8×10^{-20} calculated by Larson et al. [29] for alumina–silica interactions was considered suitable for treatment of edge-edge interactions. A value of A_H applicable to edge-face interactions was approximated by the average of the face-face and edge-edge Hamaker constants. For simplicity, a single value of $h_0=20$ Å was used in all calculations, this being in reasonable agreement with data from X-ray diffraction studies of aqueous clay platelet suspensions [30,31].

Below pH 7, Fig. 12 predicts all interaction forces to be attractive. The attractive edge-face force is demonstrated to be greater in magnitude than either the face-face or edge-edge interactions between pH 4.5 and pH 9, passing through a maximum at *ca.* pH 6 and not approaching zero until well beyond pH 10. The face-face interaction force passes from negative to positive at pH 7, and increases dramatically with decreasing pH. By contrast, the edge-edge interaction force is predicted to increase slightly until pH 7–8, beyond which it is observed to diminish in magnitude. The form and magnitude of the edge–edge interaction is, however, inconsequential on an interaction area basis.

A complete shear yield stress model additionally requires quantification of the structural properties of the kaolin suspension, namely the particle size and shape, coordination number and net orientation. The latter term is particularly important in determining the extent to which edge–face, face–face and edge–edge interactions occur as a function of suspension pH. Unfortunately, the mathematical form of the particle orientation is not obvious. The following discussion will therefore follow the qualitative assessment of Rand et al. [26]. In broad terms, at the lowest pH conditions considered in this study, most particles are anticipated to interact in an edge–face manner. However, interactions between faces will also be significant due to the large (*ca.* 10:1) ratio of the face to edge surface area. Face–face association has previously been

noted to drive formation of lamellar structured tactoids in kaolin suspensions. The result is a decrease in the suspension shear yield stress [32]. As the pH rises, the attractive face–face force is expected to diminish in magnitude (Fig. 12) and the particles will reorientate in order to allow further edge–face association to occur. The predicted result is an increase in the net interparticle attraction, and so the shear yield stress. The maximum in the edge–face interaction force at pH 6 is in good agreement with the experimental data given in Fig. 9. As the edge-face attractive force diminishes and repulsion between the kaolin faces grows, the net force is predicted to decrease rapidly. Edge–edge association is predicted to increase, but will not represent a significant force. At high pH, both the edge–face and edge–edge interaction forces approach zero. Under these circumstances, a completely dispersed ($\tau_y = 0$) suspension will result. Fig. 9 shows the onset of dispersion to occur at pH 9.5–10 for the kaolin suspensions considered in this study.

Obviously the scaled force data presented in Fig. 12 is at best a close estimate due to the approximate method of predicting the edge zeta potential behaviour as a function of pH. In the above discussion, we have considered the case of a relatively low edge charge density. For higher magnitude edge potentials, Eqs. (16)–(18) predict the edge–face interaction force to increase in magnitude relative to both the face–face and edge–edge forces. In addition, both the edge–face and edge–edge interaction forces are found to diminish more rapidly from their maximum values, indicative of the onset of dispersion at a slightly lower pH condition. Nevertheless, the net effect on the general orientation behaviour discussed previously should be small. The calculation of force data as presented in Fig. 12 is, therefore, a useful means by which to gauge the trends, but not absolute values, of the shear rheology of kaolin suspensions as a function of the suspension pH.

4. Conclusions

The approach of Hunter and others [23,24] of plotting the shear yield stress of flocculated suspensions against ζ^2 has been extended to provide information on inter-particle spacing and demonstrate the role of pair-wise interactions in controlling the rheology of spherical particulate systems. The non-linearity of the normalized kaolin yield stress versus ζ^2 data is indicative of the significant role played by particle orientation as driven by edge–face, edge–edge and face-face interaction forces. The force curves derived from consideration of electrokinetic data using the HHF treatment are of use in assessing the comparative strengths and behaviours of the kaolin edge–face, face–face and edge–edge interactions, and so allow qualitative assessment of the shear yield stress. The collapse of both the kaolin and alumina shear yield stress data to a single normalized curve demonstrates that the pair-wise interaction between particles is constant over the volume fraction range of interest. Under such circumstances, use of the semi-empirical electroacoustic volume fraction correction to the zeta potential developed by O'Brien appears reasonable.

Acknowledgment

The authors wish to thank the Australian Research Council for funding through the Advanced Mineral Products Special Research Centre and Water Services Australia for funding through the Urban Water Research Association of Australia. A special acknowledgment is given to Assoc. Prof. Robert Hunter of the University of Sydney for his contribution to the science on which much of this work is based.

References

[1] P.J. Scales, P.C. Kapur, S.B. Johnson, T.W. Healy, AIChE J., in press.
[2] P.C. Kapur, P.J. Scales, D.V. Boger, T.W. Healy, AlChE J. 43 (1997) 1171.
[3] E.J.W. Verwey, J.Th.G. Overbeek, Theory of the Stability of Lyophobic Colloids, Elsevier, Amsterdam, 1948.
[4] R. Hogg, T.W. Healy, D.W. Fuerstenau, Trans. Faraday Soc. 62 (1966) 1638–1651.
[5] A.A. Potanin, W.B. Russel, Phys. Rev. E 53 (1996) 3702.

[6] A.A. Potanin, R. De Rooij, D. Van den Ende, J. Mellema, J. Chem. Phys. 102 (1995) 5845.
[7] Z. Zhou, M.J. Solomon, P.J. Scales, D.V. Boger, The Yield Stress of Concentrated Suspensions of Mixtures of Size Distributed Particles at the Isoelectric Point, preparation.
[8] H. Iwata, T. Homma, Powder Technol. 10 (1974) 79.
[9] M. Suzuki, K. Makino, M. Yamada, K. Iinoya, Int. Chem. Engng 21 (1981) 482.
[10] R.W. O'Brien, L.R. White, J. Chem. Soc. Faraday Trans. 2 (74) (1978) 1607.
[11] R.W. O'Brien, J. Fluid Mech. 212 (1990) 81.
[12] R.W. O'Brien, J. Fluid Mech. 190 (1988) 71.
[13] Q.D. Nguyen, D.V. Boger, J. Rheol. 27 (1983) 321.
[14] Q.D. Nguyen, D.V. Boger, J. Rheol. 29 (1985) 335.
[15] P.F. Rider, R.W. O'Brien, J. Fluid Mech. 257 (1993) 607.
[16] P.F. Rider, J. Colloid Interface Sci. 172 (1995) 1.
[17] D.N. Furlong, P.A. Freeman, A.C.M. Lau, J. Colloid Interface Sci. 80 (1981) 20.
[18] P.C. Hidber, T.J. Graule, L.J. Gauckler, J. Eur. Ceramic Soc. 17 (1997) 239.
[19] G.R. Wiese, T.W. Healy, J. Colloid Interface Sci. 51 (1975) 427.
[20] R.W. O'Brien, W.N. Rowlands, R.J. Hunter, Determining Charge and Size with the Acoustosizer, in: S.G. Malghan (Ed.), Proceedings of Electroacoustics for Characterization of Particulates and Suspensions Conference: NIST Special Publication 856, National Institute of Standards and Technology, USA, 1993, p. 1.
[21] M.L. Carasso, W.N. Rowlands, R.A. Kennedy, J. Colloid Interface Sci. 174 (1995) 405.
[22] D.B. Hough, L.R. White, Adv. Colloid Interface Sci. 14 (1980) 3.
[23] R.J. Hunter, S.K. Nicol, J. Colloid Interface Sci. 28 (1968) 250.
[24] B.A. Firth, J. Colloid Interface Sci. 57 (1976) 257.
[25] D.J.A. Williams, K.P. Williams, J. Colloid Interface Sci. 65 (1978) 79.
[26] B. Rand, I.E. Melton, J. Colloid Interface Sci. 60 (1977) 308.
[27] M.D.A. Bolland, A.M. Posner, J.P. Quirk, Aust. J. Soil Res. 14 (1976) 197.
[28] P.C. Hiemenz, Principles of Colloid and Surface Chemistry, 2nd ed., Marcel Dekker, New York, 1986, p. 648.
[29] I. Larson, C.J. Drummond, D.Y.C. Chan, F. Grieser, Langmuir 13 (1997) 2019.
[30] H. Tateyama, P.J. Scales, M. Ooi, S. Nishimura, K. Rees, T.W. Healy, Langmuir 13 (1997) 2440.
[31] H. Tateyama, P.J. Scales, M. Ooi, S.B. Johnson. K. Rees, D.V. Boger, T.W. Healy, submitted to Langmuir.
[32] R.K. Schofield, H.R. Samson, Disc. Faraday Soc. 18 (1954) 135.